Second harmonic generation of guided wave at crack-induced debonding in FRP strengthened metallic plates

Yi Yang[1], Ching-Tai Ng[1,*], Andrei Kotousov[2]

[1] School of Civil, Environmental & Mining Engineering, The University of Adelaide, SA 5005, Australia

[2] School of Mechanical Engineering, The University of Adelaide, SA 5005, Australia

Abstract

The use of fibre reinforced polymer (FRP) has been widely recognised to be an effective and economical way to strengthen existing structures or repair damaged structures for extending their service life. This study investigates the feasibility of using nonlinear guided wave to monitor crack-induced debonding in FRP strengthened metallic plates. The study focuses on investigating the nonlinear guided wave interaction with the crack-induced debonding. A three-dimensional (3D) finite element (FE) model is developed to simulate the crack-induced debonding in the FRP strengthened metallic plates. The performance of using fundamental symmetric (S_0) and anti-symmetric (A_0) mode of guided wave as incident wave in the second harmonic generation at the crack-induced debonding is investigated in detail. It is found that the amplitude of the second harmonic and its variation with different damage sizes are very different when using S_0 and A_0 guided wave as the incident wave, respectively. The results suggest that it is possible to detect potential damage and distinguish its type based on the features of the generated second harmonic.

Keywords: FRP strengthening; second harmonic generation; fatigue crack; debonding; finite element simulation, nonlinear guided wave

1. Introduction

FRP strengthened aluminium plates have been widely used in aircraft structures due to its ability in fatigue crack grow resistance, high tensile strength and low density[1,2]. Meanwhile, externally bonded composite patches have also been applied to repair cracks in aircraft structures. The composite repair provides efficient load transfer and reinforcement for the structures with cracks, and thus, it prevents or retards the crack propagation[3-5].

For the FRP strengthened aluminium plates, damages, such as fatigue crack and debonding, can also be generated due to impact or fatigue loading Thus, it needs a reliable damage detection system that can detect both fatigue crack and debonding to ensure the safety and integrity of the structure. For composite repaired aluminium plates, the existing crack can still propagate under fatigue loading[7]. Meanwhile, debonding between the composite patch and damaged structure can be initiated by poor bonding or propagation of fatigue crack[8]. The debonding area can grow under loading and result in losing the strength of the reinforcement. As a result, it is necessary to monitor the integrity of the composite repair structures constantly.

1.1. Linear guided wave

Guided wave, with the ability to inspect a larger area compared with the ultrasonic bulk wave[9] and high sensitivity to small and different types of damages[10-12], provides an attractive approach for damage detection. In the last two decades, guided wave has attracted significant research interests[9,12]. In general, the studies focused on understanding the physical insights into the guided wave interaction with different types of damages, e.g. thickness reduction[13,14], crack[15,16], delamination[17-19] and debonding[20-22], and developing guided wave based damage

detection techniques using time-of-flight information of the waves[23,24], maximum-likelihood estimation[25], imaging approach[26-28], phase-array approach[29,30], model-based approach[31] and time-reversal approach[32,33] etc.

Guided wave has been used to detect and monitor damages in the metallic plates strengthened by externally bonded materials. Pavlopoulou *et al.*[34] used linear Lamb wave propagation through a notched aluminium plate bonded with an aluminium patch. The experiment showed that the crack and debonding growth under cyclic tensile loading could be monitored by their proposed damage detection method using outlier analysis. Puthillath and Rose[35] experimentally studied the adhesive and cohesive weakness on an aluminium aircraft skin repaired by a titanium repair patch using Lamb wave propagation. They observed the energy level of the received Lamb wave after propagating through the defect area. Ihn and Chang[7] carried out an experimental study using a built-in piezoelectric senor/actuator network within a composite repair patch bonded on a notched aluminium plate. They proposed to use fundamental anti-symmetric (A_0) and symmetric mode (S_0) of Lamb wave to detect the debonding and fatigue crack on the repaired material, respectively. It should be noted that of the aforementioned studies only focused on using linear guided wave, which is not as sensitive as the nonlinear guided wave in detecting incipient damages and early state of material degradations[36,37]. Also, the linear guided wave approach usually requires on reference data to extract the scattered wave information for damage detection. But the extraction of the scattered wave information through reference data could fail due to the varying environmental condition such as e.g. temperature[38,39] and loading variation[40].

1.2. Nonlinear Guided Wave induced by Contact Nonlinearity

Different to linear guided wave, nonlinear guided wave correlates the presence and characteristics of a damage with measured signals whose frequencies differ from the frequencies of the input signal to the structures. The generation of signal with different frequencies is a result of a nonlinear transformation of the input energy due to damage or other nonlinearities.

Higher harmonic generation is one of the commonly used nonlinear features. The generation of higher harmonics of contact-type defects, such as fatigue cracks, delamination and debonding, is mainly due to contact nonlinearity[42-44]. Taking fatigue crack as an example, when guided wave propagates through the fatigue crack, the compressional part of the wave closes the crack while the tensile part open it. As a result, the compression part of the wave can pass through the crack, while the tensile part cannot, and a nearly half-wave rectification of the waveform occurs after the wave passes through the crack[45]. Previous studies proved the ability of using nonlinear guided waves, typically higher harmonic generation, to detect delamination and fatigue cracks[46-49]. Soleimanpour *et al.*[48] investigated the higher harmonic generation of A_0 guided wave at a delamination in composite beams. Both experiments and FE simulations were used to provide physical insights into the higher harmonic generation due to delaminations with sizes and locations. Yang *et al.*[49] investigated the second harmonic generation in an aluminium plate with a fatigue crack. They found that S_0 guided wave is more sensitive to the fatigue crack than A_0 mode, and it can generate larger magnitude of second harmonic. They also extended the study to take investigate the second harmonic generated under practical conditions such as effect of the applied load and incident angle of the incident wave[50].

In practical situation, when the fatigue crack appears in the FRP strengthened metallic plate, it could lead to debonding between the FRP and metallic plate at the area surrounding the fatigue crack. The study of higher harmonic generation due to the combined effect of both fatigue crack and debonding in the FRP strengthened metallic plate was very limited in the literature. Most of the existing studies only considered the fatigue crack or debonding separately[51]. Therefore, this study investigates the second harmonic generation due to the interaction of guided wave at crack-induced debonding. In this study, three-dimensional (3D) finite element (FE) simulation, which was proved to be capable of providing a reliable prediction on both linear[48] and nonlinear[49] guided wave features at the damages in structures, is used to gain physical insights into the higher harmonic generation phenomenon. This study indicates the feasibility of using second harmonic generation in monitoring the propagation of fatigue crack and debonding in the FRP strengthened metallic plate.

The rest of the paper is arranged as follow. Section 2 describes the details of the 3D FE model, in which the crack-induced debonding is also described in detail. Section 3 presents the results and discussion of a series of numerical case studies using the 3D FE model. Finally, conclusions are presented in Section 4.

2. Three-dimensional finite element model

2.1. Modelling of guided wave propagation in FRP strengthened aluminium plate

A FRP strengthened aluminium plate is modelled using commercial FE software, ABAQUS. The schematic diagram of the plate model is shown in Fig. 1. The model consists of a 400mm×200mm×1.6mm aluminium plate, in which the top and bottom surface of the aluminium plate are strengthened by a 400mm×200mm×0.8mm three-ply $[0]_3$ unidirectional

composite laminate. The lamina is made by Cycom® 970/T300 unidirectional carbon/epoxy prepreg tapes with 0.55 fibre volume fraction and 0.2 mm thickness. The material properties of the lamina are shown in Table 1. In the model, the fibres of the composite laminate are all align with 1-axis direction as defined in Fig. 1. For the aluminium plate, the Young's modulus, Poisson ratio and density of the material are 70GPa, 0.33 and 2700kg/m^3, respectively.

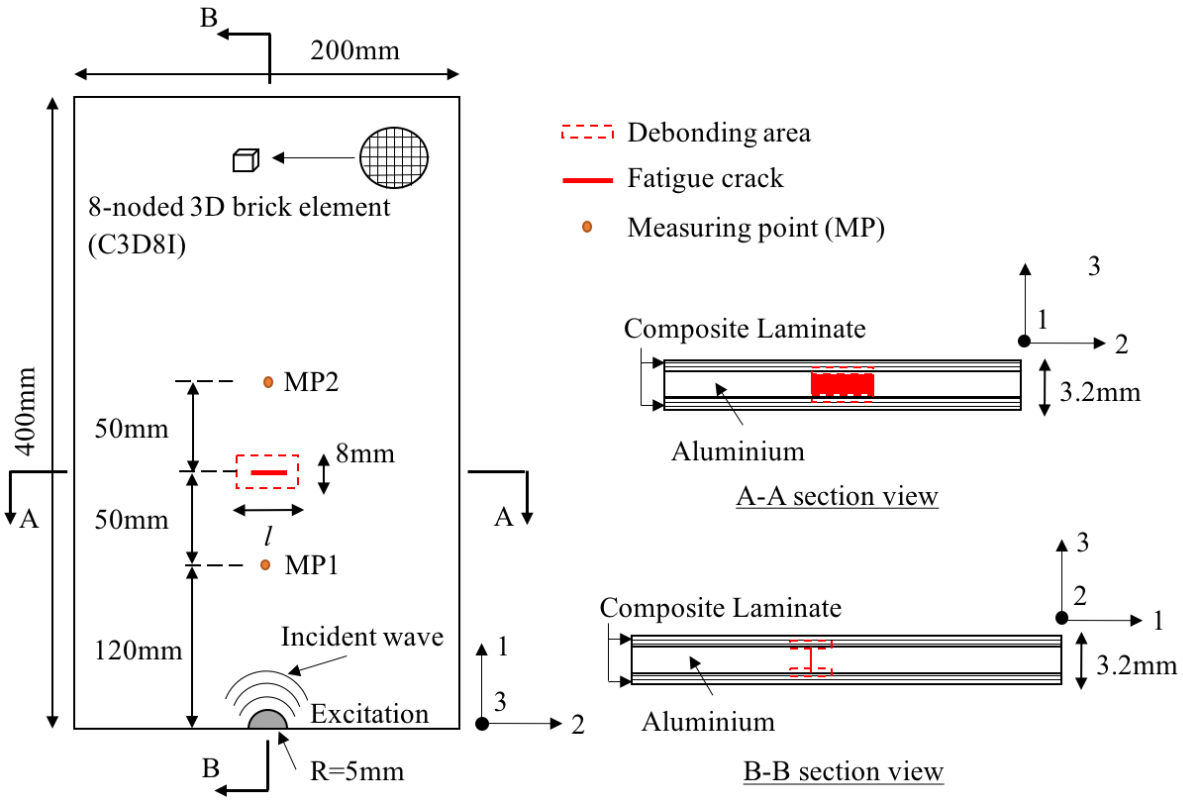

Fig. 1. Schematic diagram of the 3D FE model in ABAQUS

The incident guided wave is a 200kHz narrow-band six-cycle sinusoidal tone burst pulse modulated by a Hanning window. Fig. 2 shows the phase and group velocity disperse curves of the FRP strengthened aluminium plate obtained from DISPERSE. The figures show that only S_0 and A_0 guided wave can be excited at 200kHz. The guided wave is excited at the location of the plate as shown in Fig. 1. The guided wave is excited by applying the nodal displacement to two half circle transducer regions located at the top and bottom surface of the

plate. Both reflected and transmitted signals at the damage are measured at the measuring points MP1 and MP2 as shown in Fig. 1, respectively.

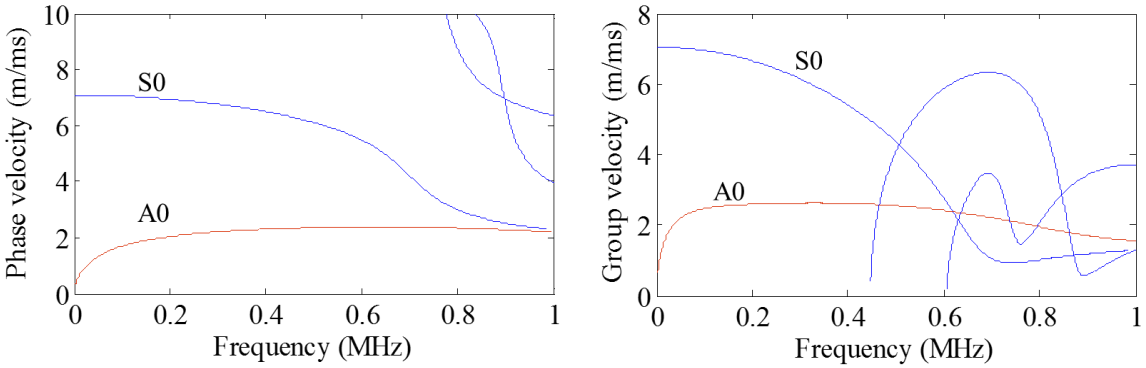

Fig. 2. Phase and group velocity dispersion curve of the 3.2mm thick FRP strengthened aluminium plate

For the excitation of S_0 guided wave, in-plane displacement is applied to the circumferences of the transducer region located at the top and bottom surface of the plate, at which the displacement is applied in radial direction as shown in Fig. 3a. While for the excitation of A_0 guided wave, out-of-plate displacement is applied to the whole surface of the transducer regions at the top and bottom surface as shown in Fig. 3b. The magnitude of the displacement is 1μm. The propagating guided wave signal is obtained at the measurement points as shown in Fig. 1. The S_0 and A_0 guided wave is measured through the strain in 1-axis and 3-axis direction as shown in Fig. 1, respectively.

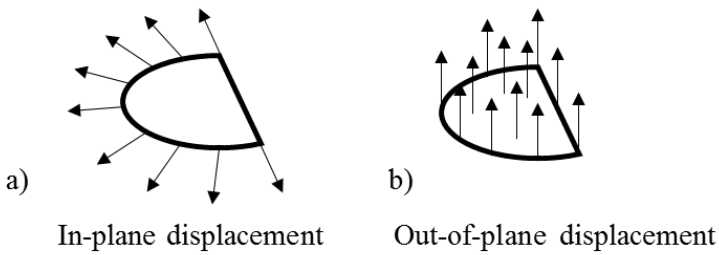

Fig. 3. Excitation of S_0 and A_0 guided wave on a half circle transducer region

Eight-noded 3D fully integrated linear brick elements, C3D8I, in which each node has three translational degrees-of-freedom (DoFs), are used to model the FRP strengthened plate. The element size is 0.4mm×0.4mm×0.4mm so the FRP strengthened plate are modelled by eight layers of elements in the through-thickness direction, in which the aluminium plate and each of the composite laminate is modelled by four and two layers of elements, respectively. In the in-plane direction, there are at least 20 elements per wavelength for the incident wave at excitation frequency, i.e. 200kHz (10mm for A_0 guided wave and 35mm for S_0 guided wave) and 10 elements per wavelength for the second harmonic guided wave at 400kHz (5mm for A_0 guided wave and 16mm for S_0 guided wave). The simulation is solved using the ABAQUS/Explicit.

2.2. Modelling of crack-induced debonding

A fatigue crack is first modelled in the aluminium plate by inserting a seam as shown in Fig. 4, which generates duplicated nodes at the pre-defined crack location as shown in Fig. 1. The composite laminate is bonded to the top and bottom surface of the aluminium plate using tie constraint at the contacting interfaces, except for the areas modelled as debonding as shown in Fig. 4. The width of the debonding is fixed at 8mm. For the fatigue crack and debonding, hard normal contact and friction tangential contact are applied to the contacting interfaces to prevent nodes penetration, and thus, simulating the clapping behaviour when the guided wave interacts with the contact-type defects. For the fatigue crack, a friction coefficient of 1.5 is used[49], and for the debonding, a friction of 0.23 coefficient is used[52].

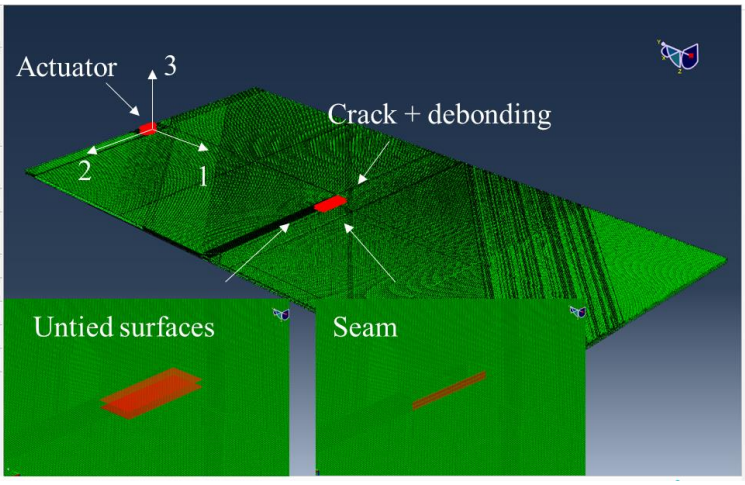

Fig. 4. FE model of the FRP strengthened aluminium plate with a 20mm long fatigue crack and two 20mm long debonding areas

Fig. 5 shows the snapshots of A_0 guided wave propagating on the model as shown in Fig. 4. Fig. 5a clearly shows that A_0 guided wave is properly excited, and the peak of the wave is in the fibre orientation of the FRP. As shown in Fig. 5b, when the wave propagate through the damage area, both reflected and transmitted wave from the damage are observed. Meanwhile, Fig. 5b also shows that the debonding and fatigue crack are opened by the guided wave.

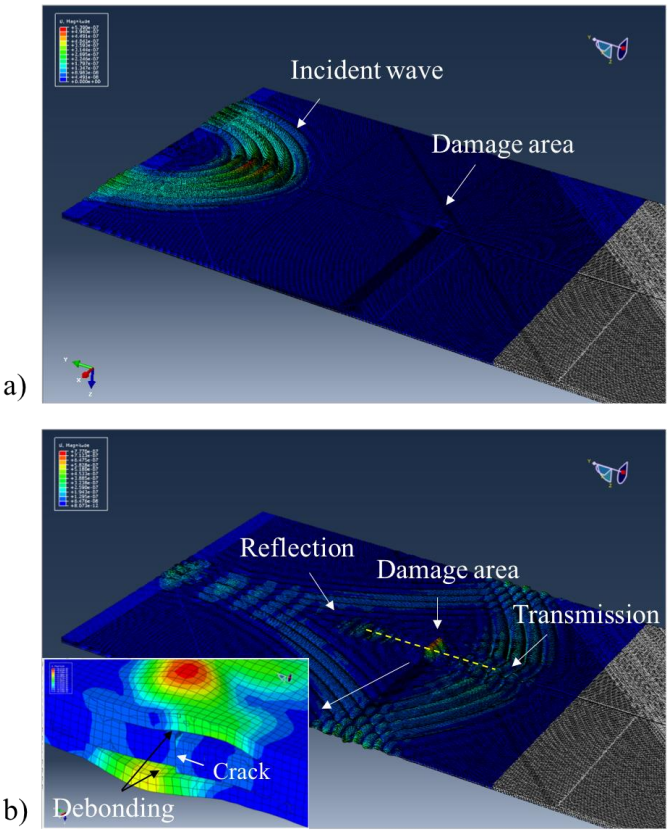

Fig. 5. Snapshots of guided wave propagation in the FRP strengthened aluminium plate with a 20mm long fatigue crack and a 20mm long debonding: a) A_0 guided wave excited by the actuator, and b) transmitted and reflected wave from the damage area and the cross-section view at the damage area.

Table 1. Material properties of Cycom® 970/T300 lamina

E_{11}(GPa)	E_{22}(GPa)	E_{33}(GPa)	G_{12}(GPa)	G_{13}(GPa)	G_{23}(GPa)	ν_{12}	ν_{13}	ν_{23}	ρ(kg/m^3)
128.75	8.35	8.35	4.47	4.47	2.90	0.33	0.33	0.44	1517

3. Case studies and discussions

A series of case studies were carried out to investigate the crack-induced debonding on the higher harmonic generation of the guided wave in the FRP strengthened aluminium plate. Three scenarios were considered in this study. In each scenario, the S_0 and A_0 guided wave

was used as incident wave, separately. Below is a summary of the scenarios considered in this study.

Scenario 1. There is no debonding between aluminium and composite laminates. Only the fatigue crack is modelled and the crack lengths considered are 8mm, 12mm, 16mm and 20mm.

Scenario 2. Both fatigue crack and debonding are modelled, and both crack lengths and debonding lengths considered are 8mm, 12mm, 16mm and 20mm.

Scenario 3. Both figure crack and debonding are modelled. The crack length is fixed at 8mm but the debonding lengths considered are 8mm, 12mm, 16mm and 20mm.

Fig. 6a shows the time-domain signal obtained at the measurement point MP1, i.e. reflected wave, from the plate with a 20mm long fatigue crack only. In Fig. 6, S_0 guided wave was used as the incident wave. The obtained time signal was processed using Short Time Fourier Transform (STFT), which provides the time-frequency information of the signal. The spectrogram parameters in the STFT were carefully selected by a series of trials to ensure the balance between time and frequency resolution. Figs. 6b and 6c show the spectrogram of the incident wave and the second harmonic wave, respectively. The results show that the second harmonic, which is reflected from the fatigue crack, arrives later than the incident wave. The arrival time of the incident wave and second harmonic wave has good agreement with the arrival time calculated based on the group dispersion curve in Fig. 2.

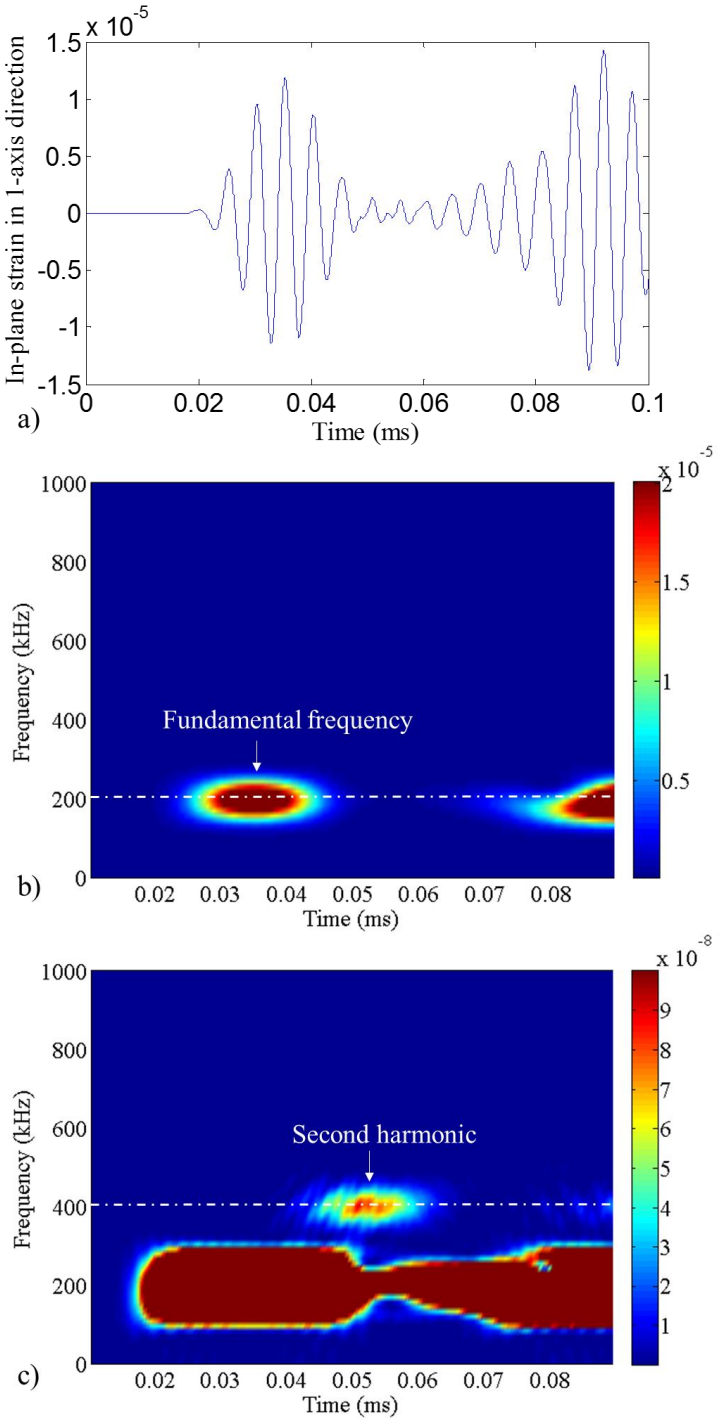

Fig. 6. Reflected S_0 guided wave obtained from the model with a 20mm fatigue crack, a) time-domain signal, b) the corresponding spectrogram, and c) spectrogram with modified colour scale for displaying the second harmonic component

The amplitude profiles of the spectrogram at 200kHz (f_0) and 400kHz ($2f_0$) were extracted and plotted in Fig. 7. The peak of the second harmonic amplitude profile was obtained and compared with the results obtained in other scenarios. The second harmonic amplitude was normalised by the maximum amplitude of the signal at fundamental frequency obtained at the damage centre location of the corresponding intact FRP strengthened plate. For Scenario 1 considering only the crack growth, the normalised second harmonic amplitude is denoted as $A_{2,c}$, while for Scenarios 2 and 3, the normalised second harmonic amplitude is denoted $A_{2,c+d}$ and $A_{2,d}$, respectively. The subscripts 'c', 'c+d' and 'd' mean the results obtained from the model with the crack only, crack and debonding, and debonding with fixed crack length, respectively.

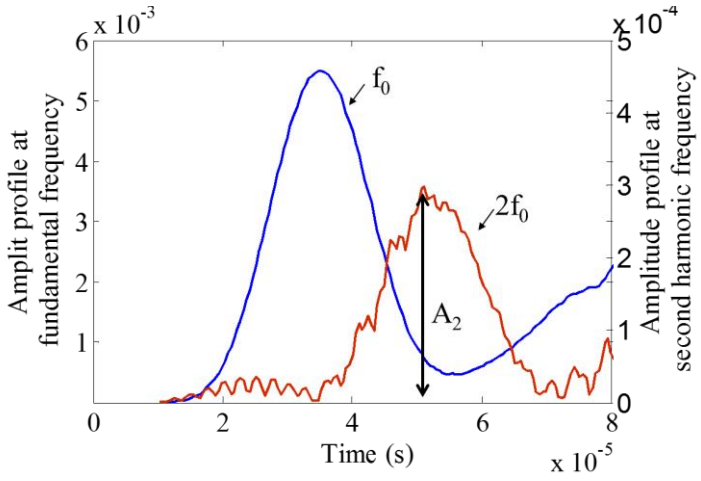

Fig. 7. Amplitude profile at fundamental frequency (blue line) and second harmonic frequency (red line) for the model with a 20mm fatigue crack and S_0 incident wave.

3.1. Scenario 1

For the Scenario 1, the model contains a fatigue crack only. Fig. 8 shows that the value of A_{2c} obtained with S_0 incident wave is higher than that of using A_0 incident wave for different

crack lengths in both reflected and transmitted signals. Meanwhile, when crack size increases, the value of $A_{2,c}$ increases monotonously of using both S_0 or A_0 guided wave as incident wave. However, when A_0 guided wave is used as the incident wave, both the magnitude and the rate of increase of $A_{2,c}$ are smaller than that of using S_0 as incident wave. The results suggest that the S_0 guided wave is more sensitive to the fatigue crack than A_0 guided wave, which is consistent with the findings in previous research[49].

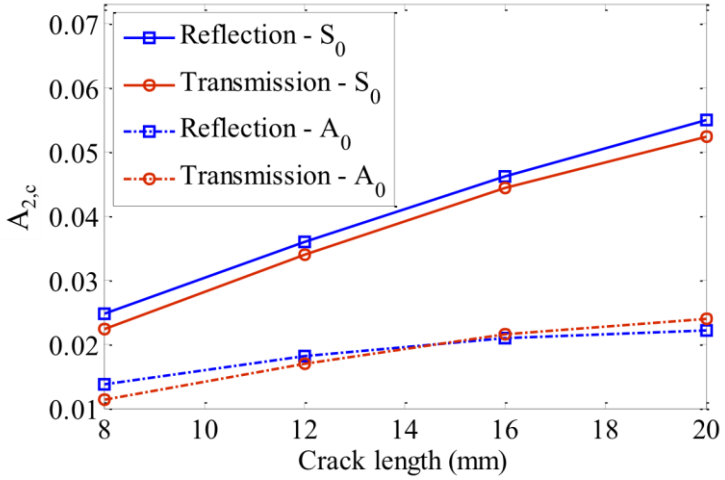

Fig. 8. Variation of normalised second harmonic with fatigue crack length for Scenario 1: the model with fatigue crack only ($A_{2,c}$)

3.2. Scenario 2

For the Scenario 2, both fatigue crack and debonding are modelled, and the length of both of them increase simultaneously. Fig. 9 shows that the value of $A_{2,c+d}$ for the reflected and transmitted wave signals increases with the fatigue crack and debonding length when S_0 and A_0 guided wave is used as incident wave, respectively. For transmitted wave, the value of $A_{2,c+d}$ for the case of using A_0 incident wave is higher than that of using S_0 incident wave. However, the value of $A_{2,c+d}$ for using S_0 incident wave is higher than that of using A_0 incident wave in the case of reflected wave. The ratio of $A_{2,c+d}$ to $A_{2,c}$ is also shown in Fig. 10, which shows the difference of the second harmonic amplitude between the model with both

crack and debonding, and crack only. Fig. 10 shows that when S_0 incident wave is used, the value of $A_{2,c+d}$ is about four times higher than $A_{2,c}$ when both fatigue crack and debonding are existed in the model. There are two reasons that the value of $A_{2,c+d}$ is larger than the $A_{2,c}$. Firstly, it can be due to the frictional contact between debonding interfaces induced by S_0 guided wave. Secondly, compared with the results of Scenario 1, when there is no debonding, the interaction of the crack interfaces is restricted by the composite patches. However, this restriction is released when the composite patches are debonded. In contrast, when A_0 guided wave is used, the $A_{2,c+d}/A_{2,c}$ ratio increases more significantly when the damage length increases, and the $A_{2,c+d}/A_{2,c}$ ratio of the transmitted wave is larger than that of reflected wave. The observations from Figs. 9 and 10 indicate that A_0 guided wave is more sensitive to debonding than S_0 guided wave. The results also show that the second harmonic guided wave induced by debonding are mainly scattered in the wave propagation direction.

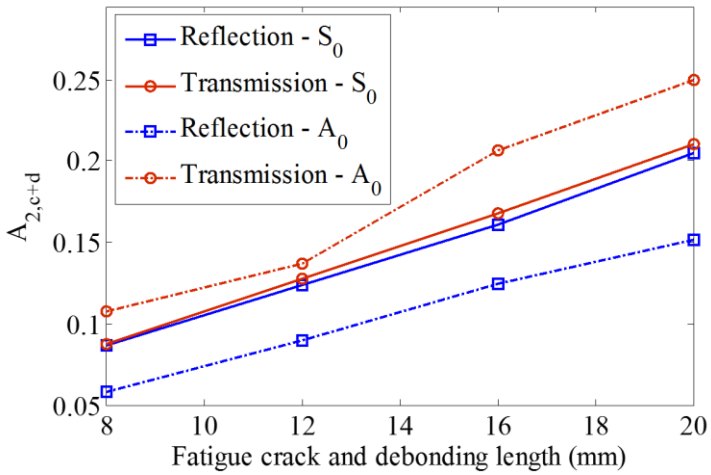

Fig. 9. Variation of normalised second harmonic with fatigue crack and debonding length on model with fatigue crack and debonding ($A_{2,c+d}$)

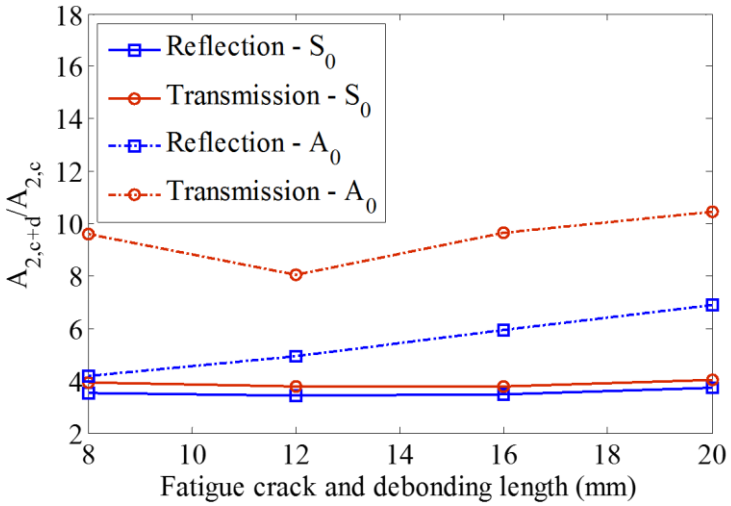

Fig. 10. Ratio of $A_{2,c+d}$ /$A_{2,c}$ for different fatigue crack and debonding lengths.

3.3. Scenario 3

For the Scenario 3, the fatigue crack length is fixed at 8mm and the debonding length increases from 8mm to 20mm. As shown in Fig. 11, when S_0 incident wave is used, the value of $A_{2,d}$ remains about the same magnitude for both transmitted and reflected wave despite the increase of the debonding length. When A_0 incident wave is used, the value of $A_{2,d}$ in the transmission direction is higher than that when S_0 incident wave is used. For the reflection direction, the $A_{2,d}$ value obtained by using S_0 incident wave is higher than that of using A_0 incident wave. Similar finding was obtained in the work of Soleimanpour *et al.*[48], in which the second harmonic amplitude varies with the delamination length without a clear trend when A_0 incident wave is used. It should be noticed that the second harmonic of the transmitted wave using A_0 incident wave is much higher than that of the reflected wave. Comparing with the results of the model with the fatigue crack only, the ratio between the $A_{2,d}$ and $A_{2,c}$ decreases when A_0 and S_0 incident wave is used, respectively, and the decreasing rate in the transmitted wave of using A_0 incident wave is more obvious (Fig. 12).

Meanwhile, the ratio of using A_0 incident wave is also higher than that of using S_0 incident wave. This is similar to the results of the Scenario 2.

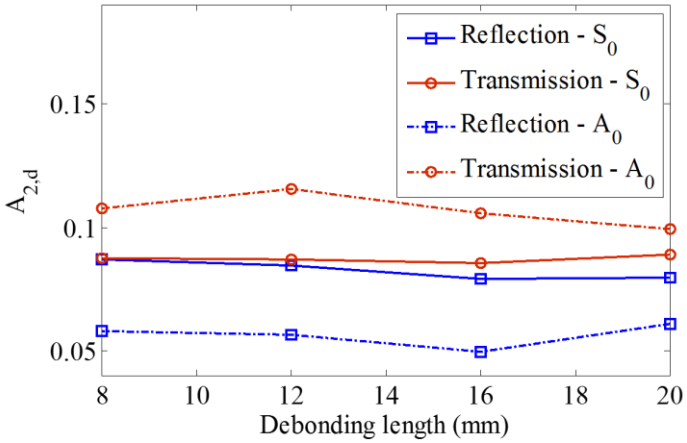

Fig. 11. Variation of normalised second harmonic with fatigue crack and debonding length for model with both fatigue crack and debonding ($A_{2,d}$)

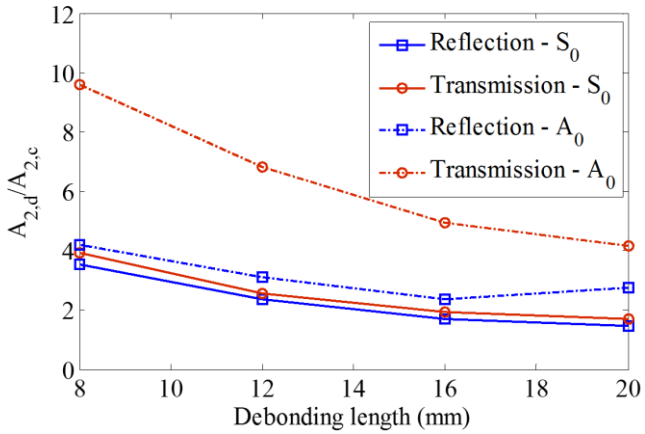

Fig. 12. Ratios of $A_{2,d}$ /$A_{2,c}$ with different debonding lengths.

4. Conclusions

This study has presented an investigation of the second harmonic generation due to guided wave interaction with the crack-induced debonding in the FRP strengthened aluminium plate. In this study, 3D FE simulations have been used to predict the wave propagation and

scattering at the crack-induced debonding in the FRP strengthened aluminium plate. Three different damage scenarios, fatigue crack only, both crack and debonding, and debonding with the fixed crack length have been considered. In each damage scenario, a six-cycle 200 kHz S_0 and A_0 incident wave have been used separately to reveal the second harmonic generation due to the contact nonlinearity.

The simulation results have shown that for different damages and different incident wave modes, the second harmonic amplitude variation against the damage length has a unique characteristic. It has been observed that S_0 incident is more sensitive for fatigue crack and A_0 incident wave is more sensitive to debonding. This indicates that normal contact is the major source of nonlinearity contributing the second harmonic generation as compared with the frictional contact. The results have also shown that when A_0 incident wave is used, the second harmonic amplitude is generally larger than that when S_0 incident wave is used for the model with debonding. In addition, when S_0 incident wave is used, the second harmonic amplitude increases only when the length of the fatigue crack increases, while the increase of debonding length will not obviously increase the second harmonic amplitude. For the model with debonding, the second harmonic amplitude of the transmitted wave is larger than that for the reflected wave, especially when A_0 incident wave is used. For the model with the fatigue crack only, the second harmonic amplitude of reflected wave is slightly larger than that of transmitted wave when S_0 incident wave is used.

These findings have shown the potential of using A_0 and S_0 guided wave in detecting and identify the damage, such as debonding or/and fatigue crack, in the FRP strengthened metallic plate. Further work can be carrying out experimental tests to study the practical feasibility of using nonlinear guided wave to detect and distinguish different types of defects in the FRP strengthened metallic plate.

5. References

1. C.T. Lin, P.W. Kao and F.S. Yang, Fatigue behaviour of carbon fibre-reinforced aluminium laminates, *Composites*, **22** (1991) 135-141.
2. S.H. Song, Y.S. Byun, T.W. Ku, W.J. Song and J Kim, Experimental and numerical investigation on impact performance of carbon reinforced aluminium laminates, *J. Mater. Sci. and Technol.* **26** (2010) 327-332.
3. C. Soutis, D.M. Duan and P. Goutas, Compressive behaviour of CFRP laminates repaired with adhesively bonded external patches, *Compos. Struct*., **45**(4) (1999) 289-301.
4. S.C. Galea, I.G. Powlesland, S.D. Moss, M.J. Konk, S.P. van der Velden, B. Stade, A.A. Baker, Development of structural health monitoring systems for composite bonded repairs on aircraft structures, *Proc. SPIE* 4327 (2001) doi: 10.1117/12.436536.
5. M. Singh and W.P. Schonberg, Bonded composite patch design for aircraft structures exhibiting cracking and corrosion, *J. Aircraft*, **42**(1) (2005) 269-274.
6. A.R. Maligno, C. Soutis and V.V Silberschmidt, An advanced numerical tool to study fatigue crack propagation in aluminium plates repaired with a composite patch, *Eng. Fract. Mech.*, **99** (2013) 62-78.
7. J.B. Ihn and F.K. Chang, Detection and monitoring of hidden fatigue crack growth using a buil-in piezoelectric sensor/actuator network: II. Validation using riveted joints and repair patches', *Smart Mater. Struct.*, **13** (2003) 621-630.
8. Y. Huang, J. Liu, X. Huang, J. Zhang and G. Yue, Delamination and fatigue crack growth behaviour in Fibre Metal Laminates (Glare) under single overloads, *Int. J. Fatigue*, **78** (2015) 53-60.
9. J.L. Rose, A baseline and vision of ultrasonic guided wave inspection potential, *J. Press. Pess. technol.*, **124**(3) (2002) 273-282.
10. C. Haynes and M. Todd, Enhanced damage localization for complex structures through statistical modelling and sensor fusion, *Mech. Syst. Sig. Process.*, **54-55** (2015) 195-209.
11. S. He and C.T. Ng, A probabilistic approach for quantitative identification of multiple delaminations in laminated composite beams using guided waves, *Eng. Struct.*, **127** (2016) 602-614.
12. M. Mitra and S. Gopalakrishnan, Guided wave based structural health monitoring: A review, *Smart Mater. Struct.*, **25**(5) (2016) 053001
13. L. Moreau, M. Caleap, A. Velichko and P.D. Wilcox, Scattering of guided waves by through-thickness cavities with irregular shapes, *Wave Motion*, 48 (2011) 586–602.
14. R. Howard and F. Cegla, Detectability of corrosion damage with circumferential guided waves in reflection and transmission, *NDT&E Inter.*, **91** (2017) 108-119
15. P. Rajagopal and M Lowe, Scattering of the fundamental shear horizontal guided wave by a part-thickness crack in an isotropic plate, *J. Acoust. Soc. Am.*, **124**(5) (2008) 2895-2904.
16. S. He and C.T. Ng, Guided wave-based identification of multiple cracks in beams using a Bayesian approach, *Mech. Syst. Sig. Process.*, **84** (2017) 324-345.
17. N. Guo and P. Cawley, The interaction of Lamb waves with delaminations in composite laminates. *J. Acoust. Soc. Am.*, **94**(4) (1993) 2240-2246.
18. T.E. Michaels, J.E. Michaels and M. Ruzzene, Freqwuency-wavenumber domain analysis of guided wavefields, *Ultrasonics.*, **51** (2011) 452-466.
19. C.T. Ng, On accuracy of analytical modeling of Lamb wave scattering at delaminations in multilayered isotropic plates. *Int. J. Str. Stab. Dyn.*, **15** (2015) 1540010.

20. B. Eckstein, M.M. Bonet, M. Bach and C.P. Fritzen, Lamb wave interaction at debondings due to impact damage in complex stiffened CFRP structures, *Proc. SPIE*, **10170** (2017) 101701Q.
21. H. Mohseni and C.T. Ng, Rayleigh wave for detecting debonding in FRP-retrofitted concrete structures using piezoelectric transducers, *Compos. Concrete*, **20**(5) (2017) 583-593.
22. H. Mohseni and C.T. Ng, Rayleigh wave propagation and scattering characteristics at debondings in FRP-retrofitted concrete structures. *Struct. Health Monitor.* (2018) https://doi.org/10.1177/1475921718754371
23. S.T. Quek, P. Tua and Q. Wang, Detecting anomalies in beams and plate based on the Hilbert-Huang transform of real signals, *Smart Mater. Struct.*, **12**(3) (2003) 447.
24. D. Dai and Q. He. Structure damage localization with ultrasonic guided waves based on a time-frequency method, *Sig. Process.*, **96** (2014) 21-28.
25. E.B. Flynn, M.D. Todd, P.D. Wilcox, B.W. Drinkwater and A. J. Croxford, Maximum-likelihood estimation of damage location in guided-wave structural health monitoring, *Proc. R. Soc.*, A **467** (2011) 2575-2596.
26. C.T. Ng, A two-stage approach for quantitative damage imaging metallic plates using Lamb waves, *Earthq. Struct*., **8**(4) (2015) 821-841.
27. P. Aryan, A. Kotousov, C.T. Ng and B.S. Cazzolato (2017). A baseline-free and non-contact method for detection and imaging of structural damage using 3D laser vibrometery. *Struct. Control Health Monitor.*, **24**(4) (2017) e1894.
28. G.T. Pudipeddi, C.T. Ng and A. Kotousov, Effect of central and non-central frequency components on the quality of damage imaging. *J. Civil Struct. Health Monitor*., 8(1) (2018) 49-61.
29. L. Yu and V. Giurgiutiu, In situ 2-D piezoelectric wafer active sensors arrays for guidd wave damage detection. *Ultrasonics*, **48**(2) (2008) 117-134.
30. J.H. Han and Y.J. Kim, Time-frequency beamforming for non-destructive evaluations of plate using ultrasonic Lamb wave, *Mech. Syst. Sig. Process.*, **54-55** (2015) 336-356.
31. P. Aryan, A. Kotousov, C.T. Ng and B. Cazzolato, A model-based method for damage detection with guided waves, *Struct. Contr. Health Monitor*., **24** (2017) e1884.
32. H. Sohn, H.W. Park, K.H. Law and C.R. Farrar, Damage detection in composite plates using an enhanced time reversal method, *J. Aerospace Eng.*, **20** (2007) 141-151.
33. B. Xu and V. Giurgiutiu, Single mode tuning effects on Lamb wave time reversal with piezoelectric wafer active sensors for structural health monitoring, *J. Nondestructive Eva.*, **26**(2-4) (2007) 123-134.
34. S. Pavlopoulou, C. Soutis and G. Manson, Non-destructive inspection of adhesively bonded patch repairs using Lamb waves, *Plastics, Rubber and Compos.*, **41**(2) (2012) 61-68.
35. P. Puthillath and J.L. Rose, Ultrasonic guided wave inspection of a titanium repair patch bonded to an aluminium aircraft skin, *Int. J. Adhesion Adhesives*, **30** (2010) 566-573.
36. C. Bermes, J.Y. Kim, J. Qu and L.J. Jacobs, Nonlinear Lamb waves for the detection of material nonlinearity, *Mech. Syst. Sig. Process.*, **22**(3) (2008) 638-646.
37. M. Hasanian and C.J. Lissenden, Second order harmonic guided wave mutual interactions in plate: vector analysis, numerical simulation, and experimental results, *J. Applied Phys*, **122**(8) (2017) 084901.
38. A. Marzani and S. Salamone, Numerical prediction and experimental verification of temperature effect on plate waves generated and received by piezoceramic sensors, *Mech. Syst. Sig. Process*, 30 (2012) 204–217.

39. P. Aryan, A. Kotousov, C.T. Ng and S. Wildy, Reconstruction of baseline time-trace under changing environmental and operational conditions, *Smart Mater. Struct.*, 25(3) (2016) 035018.
40. M. Mohabuth, A. Kotousov and C.T. Ng, Effect of uniaxial stress on the propagation of higher-order Lamb wave modes. *Int. J. Nonlinear Mech.*, 86 (2016) 104-111.
41. M. Mohabuth, A. Kotousov, C.T. Ng, L.R.F. Rose, Implication of changing loading conditions on structural health monitoring utilising guided wave. *Smart Mater. Struct.*, 27(2) (2018) 025003.
42. K.Y. Jhang, Nonlinear ultrasonic techniques for non-destructive assessment of mirco damage in material: A review, *Int. J. Precision Eng. Manufacture.*, **10**(1) (2009) 123-135.
43. D. Broda, W.J. Staszewski, A. Martowicz, T. Uhl, V.V. Silberschmidt, Modelling of nonlinear crack-wave interactions for damage detection based on ultrasound – a review, *J. Sound Vib*., **333**(4) (2014) 1097-1118.
44. R. Soleimanpour and C.T. Ng, Locating delaminations in laminated composite beams using nonlinear guided waves, *Eng. Struct*., **131** (2017) 207-219.
45. S. He and C.T. Ng, Modelling and analysis of nonlinear guided waves interaction at a breathing crack using time-domain spectral finite element method, *Smart Mater. Struct.*, **26** (2017) 085002.
46. M. Hong, Z. Su, Q. Wang, L. Cheng and X. Qing, Modelling nonlinearities of ultrasonic waves for fatigue damage characterization: Theory, simulation, and experimental validation, *Ultrasonics.*, **54** (2014) 770-778.
47. H.J. Lm, B. Song, B. Park, H. Sohn, Noncontact fatigue crack visualization using nonlinear ultrasonic modulation, *NDT&E Inter*. **73** (2015) 8-14.
48. R. Soleimanpour, C.T. Ng and C.H. Wang, Higher harmonic generation of guided waves at delaminations in laminated composite beams, *Struct. Health Monit*., **16**(4) (2017) 400-417.
49. Y. Yang, C.T. Ng, A. Kotousov, H. Sohn and H.J. Lim, Second harmonic generation at fatigue cracks by low-frequency Lamb waves: Experimental and numerical studies, *Mech. Syst. Sig. Process.*, **99** (2018) 760-773.
50. Y. Yang, C.T. Ng and A. Kotousov, Influence of crack opening and incident wave on second harmonic generation of Lamb wave. *Smart Mater. Struct*. 27 (2018) 055013.
51. Y. Wang, R. Guan and Y. Lu, Nonlinear Lamb waves for fatigue damage identification in FRP-reinforced steel plates, *Ultrasonics*, **80** (2017) 87-95.
52. J. Schon, Coefficient of friction for aluminium in contact with a carbon fibre epoxy composite, *Tribol. Int.*, **34** (2003) 395-404.